

Structural Degradation of High Voltage Lithium Nickel Manganese Cobalt Oxide (NMC) Cathodes in Solid-State Batteries and Implications for Next Generation Energy Storage

Nathan D. Phillip,^{1,2} Andrew S. Westover,² Claus Daniel,^{1,3} Gabriel M. Veith^{2*}*

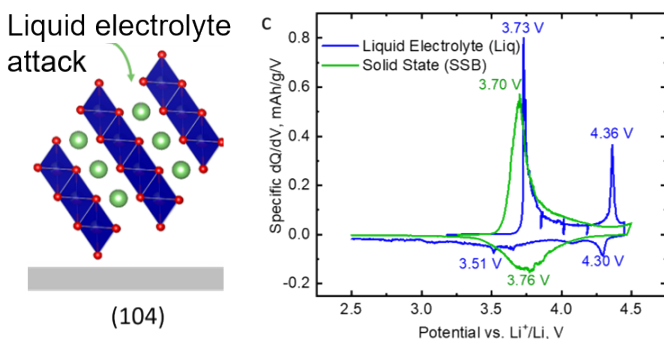
¹ The Bredesen Center for Interdisciplinary Research and Graduate Education, University of Tennessee, Knoxville, TN, 37996, USA

²Chemical Sciences Division, Oak Ridge National Laboratory, Oak Ridge, TN 37831, USA

³Energy and Environmental Sciences Directorate, Oak Ridge National Laboratory, Oak Ridge, TN 37831, USA

This manuscript has been authored by UT-Battelle, LLC, under contract DE-AC05-00OR22725 with the US Department of Energy (DOE). The US government retains and the publisher, by accepting the article for publication, acknowledges that the US government retains a nonexclusive, paid-up, irrevocable, worldwide license to publish or reproduce the published form of this manuscript, or allow others to do so, for US government purposes. DOE will provide public access to these results of federally sponsored research in accordance with the DOE Public Access Plan (<https://energy.gov/downloads/doe-public-access-plan>).

GRAPHICAL ABSTRACT



ABSTRACT

In this study we report the stability of the layered high voltage cathode NMC622 with respect to a standard liquid electrolyte and in an all solid-state configuration. NMC622 cathodes with a (104) orientation were found to suffer from degradation at high voltage (4.5V vs. Li/Li⁺) due to electrolyte promoted degradation of the layered structure; the Lipon layer was able to suppress the extent of this decomposition but not totally prevent it from occurring. In the solid-state cells the capacity decreased from 203 mAh/g to 93 mAh/g in the first cycle and from 93 mAh/g to 79 mAh/g over the subsequent 99 cycles whereas after twenty cycles the liquid cell charge capacity was dominated by the irreversible electrolyte degradation. The interfacial resistance of the solid-state cells was stable with cycling, suggesting minimal degradation of the NMC622/Lipon interface and incumbent losses due to structural evolution associated with cathode orientation. This data indicates that accessing stable high voltage capacity in NMCs will not be enabled by simply stabilized the cathode-electrolyte interface. Optimizing cathode crystallographic orientation may be the key to accessing this high voltage regime.

INTRODUCTION

Solid state batteries are predicted to be one of the next generation energy storage technologies that are inherently safer than standard Li-ion liquid electrolyte chemistries. They also have the potential for higher energy densities due to the use of Li metal and high voltage operation greater than 4.4 V vs. Li/Li⁺.¹ Ni-rich LiNi_xMn_yCo_zO₂ (NMC, where $x + y + z = 1$ and $x > 0.5$) cathodes are considered a potential next step to achieve higher energy density batteries but it remains an open question whether they are viable for high voltage (≥ 4.5 V vs. Li/Li⁺) solid state batteries.

While cycling to such high upper cutoff voltages allows for high energy density (>200 mAh/g) in Ni-rich NMC batteries, it also induces electrolyte decomposition in conventional carbonate electrolytes, possibly due to oxygen evolution from the lattice during structural rearrangement.^{2, 3} Solid state electrolytes which are intrinsically stable in this voltage regime, such as Lipon (>5.0 V stability window⁴) might offer a means to stabilize the system to take full advantage of the material.

Several studies have focused on slurry casting composite electrodes mixed with solid electrolytes such as β -Li₃PS₄, Li_{6.4}La₃Zr_{1.4}Ta_{0.6}O₁₂, Li_{1.5}Al_{0.5}Ti_{1.5}(PO₄)₃, and Li_{1.5}Al_{0.5}Ge_{1.5}(PO₄)₃.⁵⁻⁹ These works have highlighted the challenges of NMC622 and NMC811 solid state batteries including the formation of an unstable cathode/electrolyte interphase (CEI) layer against β -Li₃PS₄ which caused large first cycle capacity losses (~30%) and a continuous rise in cell impedance.⁵ A study of NMC622 slurry cast on an Li_{6.4}La₃Zr_{1.4}Ta_{0.6}O₁₂ solid electrolyte pellet with Li₃BO₃ as a sintering agent reported large first cycle capacity losses of 34 – 45% and continuously low coulombic efficiency (55 – 70%) when cycled to 4.2 V vs. Li/Li⁺.⁹ They attributed these capacity losses to microcrack formation at the interfaces.⁹ Others found that a phosphate electrolyte – Li_{1.5}Al_{0.5}Ti_{1.5}(PO₄)₃ – had no detrimental side reactions, due to higher oxidative stability of the electrolyte, although substantial capacity loss was still observed.⁷ The cause of these capacity losses may be due to structural rearrangement at the surface of Ni-rich NMCs, which is exacerbated at higher states of charge (≥ 4.5 V vs. Li/Li⁺ for NMC622). These previous studies of Ni-rich solid state batteries used composite cathodes comprised of binders and conductive carbon with dual electrolytes to stabilize the interfaces.⁶⁻⁸ The complex nature of these composite cathodes make it difficult to isolate materials challenges and interfacial reactions, and can exacerbate the challenges of mechanical damage and contact loss between the active material and solid electrolyte.^{9, 10}

Thin film batteries provide a means to separate issues with using a composite cathode from challenges of the active cathode material itself. It also provides a geometry with a well-defined electrode/electrolyte interfaces.¹¹ Previous work demonstrated the ability to use magnetron sputtering to synthesize dense planar NMC622 thin films which were stable up to 4.2 V vs. Li/Li⁺ in a standard carbonate electrolyte (1.2 M LiPF₆ in ethylene carbonate and ethyl methyl carbonate).¹²

In this work, the first Ni-rich NMC thin film battery with a Lipon electrolyte and Li anode was compared to a conventional liquid cell with thin film electrodes cycled to 4.5 V. The simplified geometry allowed for isolated study of the cathode material which was not stabilized by the solid electrolyte and suffers from structural degradation with the same loss in capacity as the liquid cell. This indicated intrinsic limitations of the NMC622 structure at high states of delithiation which were not remedied by a stable cathode/electrolyte interface.

METHODS

Synthesis. Thin films of $\text{LiNi}_{0.6}\text{Mn}_{0.2}\text{Co}_{0.2}\text{O}_2$ (NMC622) were prepared by radio frequency magnetron sputtering off home-built NMC622 targets.¹³ Deposition conditions in this study included a base chamber pressure $<2 \times 10^{-6}$ Torr with 55.0 sccm high purity Ar gas (Airgas – 99.9995%) providing 6.0 mTorr deposition pressure at 90 W. Following deposition of 1.5 μm NMC622 on a 1 cm^2 area of polished Al_2O_3 substrates coated with 10 nm Co and 250 nm Pt, thin films were annealed at 700°C for 1 h our under high purity air flow (~ 0.2 LPM, Airgas) with a ramp rate of 5 °C/min then stored in an Ar-filled glove box. Lipon films were deposited by RF sputtering of a Li_3PO_4 target (99.95% pure, Kurt J. Lesker) under 20 sccm N_2 at 20 mTorr and 90 W for 1.7 μm . A 3 μm layer of Li metal was deposited on the Lipon layer using a custom built evaporation chamber. All film thicknesses were estimated using a quartz crystal microbalance to measure deposition rates.

Characterization. X-ray diffraction (XRD) was conducted on a Scintag XDS 2000 at a standard operating mode of 45 kV and 32 mA with a $\text{Cu K}\alpha_1$ monochromated radiation source ($\lambda = 1.5406$ Å) across a $\Theta:2\Theta$ scan range of 10° – 80°. Cycled cells were extracted in an Ar-filled glove box and covered with Kapton tape to prevent air exposure.

Electrochemical Measurements. Solid state cells were sealed in stainless steel vessels in an Ar-filled glove box. Electrochemical cells with liquid electrolyte were assembled in an Ar-filled glove box in coin cells with one wave spring, one stainless steel spacer, and one 1.5 μm NMC622 thin film vs. Li metal (1 cm diameter). Two 1.3 cm diameter separators (Dreamweaver Gold 40) were placed between electrodes and soaked in 300 μL 1.2 M LiPF_6 in ethylene carbonate (EC) and ethyl methyl carbonate (EMC) in a 3:7 wt. ratio (Tomiyama). Cells rested at open circuit voltage

for 2 hours before being cycled from 2.5 – 4.5 V vs. Li/Li⁺ in a constant current, constant voltage protocol (CC/CV). The first cycle charge and discharge rates were 3 μA (5 mA/g) whereas subsequent cycles were charged and discharged at 10 μA (16.7 mA/g). The upper cutoff voltage (4.5 V) was held until the measured current dropped below 1 μA. All cells were tested at least in duplicate. Electrochemical Impedance Spectroscopy (EIS) tests were conducted with a potentiostat/galvanostat with frequency response analyzer (BioLogic). Cells were at open circuit voltage after charging to 4.5 V vs. Li/Li⁺ with a 6 mV applied signal over 10 mHz to 1 MHz for solid state cells and 10 mHz to 20 kHz for cells with liquid electrolyte with an average of 3 measurements per frequency. Impedance measurements were collected before and after the first cycle ($\pm 3 \mu\text{A}$) then after every other cycle at $\pm 10 \mu\text{A}$.

RESULTS & DISCUSSION

Additional Li⁺ inventory can be accessed by cycling intercalation cathodes to higher upper cutoff voltages (*i.e.* ≥ 4.5 V vs. Li/Li⁺), but this high voltage operation often induces structural degradation and electrolyte decomposition.^{14, 15} In the case of Ni-rich NMC, surface structural rearrangement caused by high delithiation may release reactive oxygen species which contribute to electrolyte oxidation and the buildup of degradation products at the cathode surface in carbonate electrolytes.^{2, 3, 14} This surface layer can impede Li⁺ diffusion into the cathode and the phase change can reduce the number of available Li sites for reintercalation, lowering the effective capacity of the cell at high upper cutoff voltages. Lipon is stable at these high voltages¹⁶ and so offers the potential to stabilize the CEI for long term operation. The cathodes grown in this work have a preferential texturing in the 104 orientation. As we will show we believe this orientation plays a significant role in the electrochemical results and provides a pathway to optimize cathode chemistry for the best interfacial chemistry and capacity retention.

Figure 1a shows the specific capacity of a NMC622 half cell with liquid electrolyte (1.2 M LiPF₆ in EC:EMC 3:7 wt.) cycled to 4.5 V vs. Li/Li⁺ at a current density of ± 5 mA/g for the first cycle and ± 17 mA/g for the second cycle in a constant current/constant voltage protocol (CC/CV). The first charge specific capacity reached 274 mAh/g which exceeded the theoretical specific capacity of 200 mAh/g; the first cycle discharge (193 mAh/g) was closer to theoretical. This difference between theoretical and measured capacity as well as the irreversible capacity loss between the

first charge and discharge suggest undesirable side reactions and structural degradation may be involved. The solid-state cell was in better agreement with literature, having a first cycle specific capacity of 203 mAh/g ($81.3 \mu\text{Ah}/(\text{cm}^2 \cdot \mu\text{m})$), Figure 1b. A 48% capacity drop between the first charge and discharge cycle, measured for the solid-state cell, indicated irreversible structural changes occurred during the first charge cycle.

Interestingly, the voltage profile of the two types of cells show subtle differences due to the electrolyte (liquid vs. solid). In the aprotic electrolyte the cell demonstrates a sloping plateau around 3.6 V as expected for the $\text{Ni}^{2+}/\text{Ni}^{4+}$ redox couple, but a second characteristic voltage at ~ 4.4 V. Within the solid-state cell only one sloping $\text{Ni}^{2+}/\text{Ni}^{4+}$ redox plateau can be seen in Figure 1c as a single sharp peak for the solid state cell at 3.7 V on the charge cycle and 3.8 V on discharge. The first and second cycles of a solid state NMC622/Lipon/Li cell are shown in Figure 1b at the same current densities, voltage window, and CC/CV protocol as the liquid electrolyte cell. The 4.4V plateau observed with the liquid electrolyte likely corresponds to side reactions induced by structural rearrangement of the cathode.¹⁴ This latter plateau appeared to a lesser extent on the first discharge curve at ~ 4.3 V, seen in the differential capacity plot in Figure 1c. This suggests the reaction was partially reversible and indicated a phase change and may be due to partial oxygen redox at high states of charge.¹⁵ This 4.4 V plateau is not observed on the second charge cycle (17 mA/g) nor on subsequent cycles, indicating that this plateau is correlated with an irreversible change in the cathode material which might explain the observed capacity loss and will be discussed below with the XRD data. The $\text{Ni}^{2+/4+}$ The shape of the solid-state cell voltage profile was preserved at the higher current rate of 17 mA/g, however the suppressed Ni redox plateau lead to a low second cycle specific charge capacity of 93 mAh/g. This loss of available lithium sites for reintercalation into the NMC622 cathode was similar to the 30% capacity loss after the first charge cycle in the liquid cell.

Interestingly, the specific discharge capacity of the liquid cell and solid cell were almost identical during the extended cycling experiment shown in Figure 1d at 34 and 35 mAh/g at 17 mA/g, respectively, on cycle 10. This indicated that the capacity loss mechanism is likely the same in both cells and therefore independent of electrolyte composition. This suggests that the capacity loss at high voltages is an intrinsic limitation of the NMC622 cathode itself. The steep capacity loss of 54% between charge cycles of the solid-state cell stabilized to an average coulombic

efficiency of 97% after cycle 2. While the specific charge capacity of the solid-state cell was 30.6 mAh/g at the 97th cycle, the coulombic efficiency improved to 99.2%. This minimal capacity loss during extended cycling means that following the initial structural degradation, little structural degradation or electrolyte decomposition took place, which was expected for Lipon at high voltages.⁴ Some of this capacity was rate limited, as the specific charge capacity in the 100th cycle increased to 78.8 mAh/g ($31.5 \mu\text{Ah}/(\text{cm}^2 * \mu\text{m})$) at 3 μA . We will demonstrate below that these losses are due to cathode degradation impeding ion transport to and from the NMC622 not the growth of interfacial impedance.

Conversely, the specific charge capacity of the liquid electrolyte cell first decreased before increasing steeply due to continuous electrolyte consumption. The specific charge capacity rose starting at cycle 9 while the discharge capacity remained around 33 mAh/g. This low coulombic efficiency of the liquid cell indicated an irreversible reaction occurred during the charge cycle which increased until the liquid cell was unable to reach 4.5 V at the same charge rate (after cycle 22, as seen in Figure S1). This suggested an unstable CEI which continuously consumed the liquid electrolyte until cell failure and will be discussed with AC impedance data below.

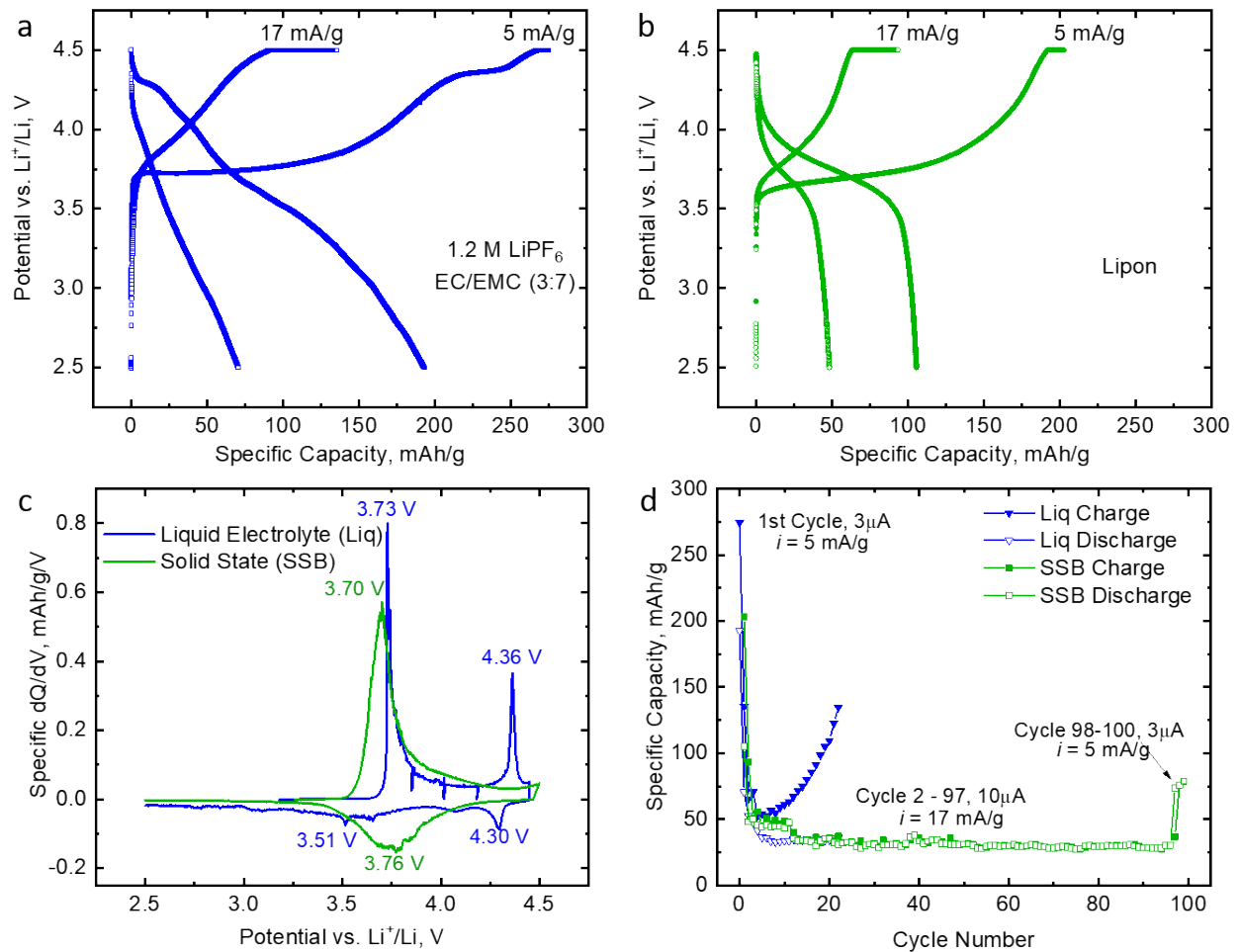


Figure 1. Specific capacity of a) liquid carbonate electrolyte cell and b) solid state cell with a constant current/constant voltage cycling protocol at ± 5 mA/g ($\sim C/40$) and ± 17 mA/g ($\sim C/12$) current densities for the first and second cycles, respectively with c) differential capacity for the liquid and solid cells at 5 mA/g and d) extended cycling at 17 mA/g until cycle 98 where the current density was returned to 5 mA/g. All cells were cycled in duplicate.

The evolution of the liquid electrolyte cells and solid-state cells was investigated using AC impedance spectroscopy. Figure 2a shows EIS data of a liquid cell from the uncycled state through the last cycle before cell failure. Following bulk electrolyte resistance (R_e) at the highest frequency, a depressed semicircle in the high frequency regime is assigned to the CEI impedance (R_{CEI}) and capacitance (Q_{CEI}), charge transfer resistance (R_{ct}), double layer capacitance (Q_{dl}) and a low frequency linear component corresponds to a finite diffusion constant phase element (Q_b) as shown in the equivalent circuit model of Figure 2a. While some examples in literature separately quantify

R_{ct} and R_{CEL} , in practice these effects are challenging to quantitatively decouple and so are reported as a single value of interfacial impedance here. The interfacial impedance of the liquid cell increased from 251 $\text{Ohm}\cdot\text{cm}^2$ to 1037 $\text{Ohm}\cdot\text{cm}^2$ after the first cycle at 5 mA/g and gradually increased to 2019 $\text{Ohm}\cdot\text{cm}^2$ after 8 cycles at 17 mA/g. This 9th cycle correlates to the increasing first cycle specific charge capacity seen in Figure 1c. This value continued to grow with this increasing capacity until it reached $\sim 5000 \text{ Ohm}\cdot\text{cm}^2$ right before cell failure (Figure S2). This continuous buildup of charge transfer resistance coupled with the increasing charge capacity with low discharge capacity observed in Figure 1d suggests continual growth of the CEI layer with cycling in the liquid electrolyte. This CEI is comprised of inorganic species from salt decomposition (e.g. $\text{Li}_x\text{PO}_y\text{F}_z$, LiF) and organic species from solvent decomposition (e.g. polycarbonates, alkyl carbonates), as detected by XPS previously.¹⁷

By contrast, the impedance data for a solid-state cell remained relatively stable over the same cycles as the liquid cell, as shown in Figure 2b. The interfacial resistance in the case of the solid state cell is a convolution of the resistance of the solid electrolyte and the electrolyte/electrode interfaces, with typical values for Lipon being 100 – 500 $\text{Ohm}\cdot\text{cm}^2$ in LiCoO_2 cells.¹¹ In this case, a high frequency semicircle corresponded to Lipon and the Lipon/NMC622 interfacial resistance and capacitance. This semicircle was more well defined than the liquid cell – reaching the x-axis before transitioning into an $\sim 80^\circ$ diffusion tail – which is characteristic of a charge transfer limited process.¹⁸ The growth of the total resistance was much less severe than the liquid cell, increasing modestly from 307 $\text{Ohm}\cdot\text{cm}^2$ for the pristine cell to 476 $\text{Ohm}\cdot\text{cm}^2$ at cycle 97. A magnified view of the high frequency semicircle is shown in the inset of Figure 2b and additional impedance data for cycles 10 – 97 are included in Figure S3. These results, coupled with the increasing coulombic efficiency with cycling, demonstrate that the NMC622/Lipon interface is more stable during high voltage cycling than the liquid electrolyte after structural failure.

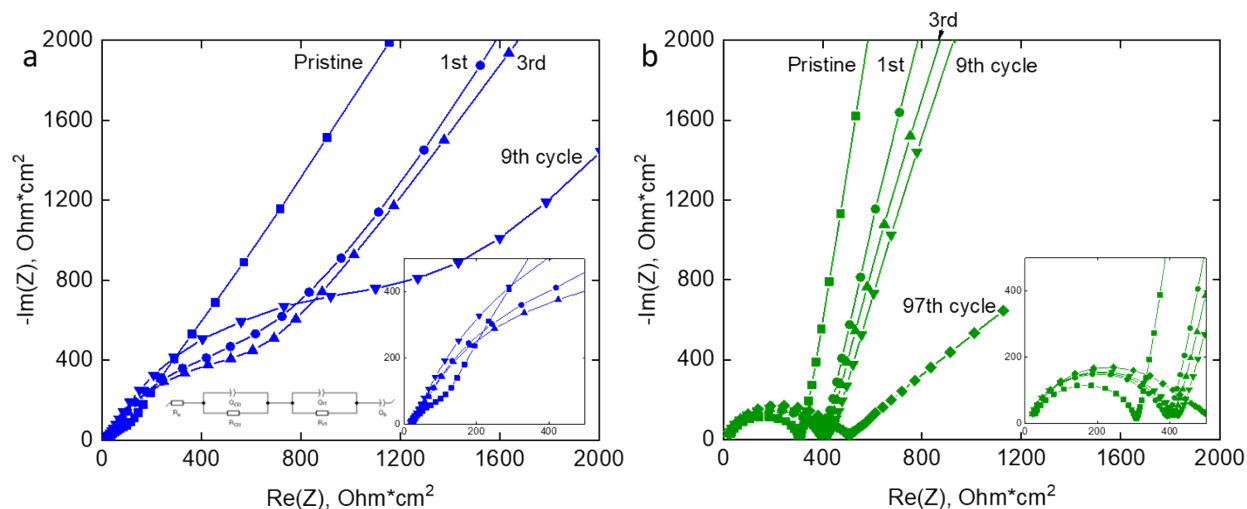


Figure 2. AC impedance of uncycled and cycled a) liquid carbonate electrolyte cell and b) solid state cell with insets showing the high frequency regimes for each sample and the equivalent circuit model used

To further confirm and elucidate the structural degradation of the NMC cathodes upon cycling, we performed XRD. The crystal structure of the NMC622 electrodes changes dramatically after cycling, as seen in the XRD spectra of Figure 3. The pristine 1.5 μm NMC622 film (in black) had distinct diffraction peaks for the Pt and Co-coated Al_2O_3 substrates, the spectrum of which is included in Figure S4. Due to the limited amount of cathode material and limited instrument resolution, only the (003), (101), and (104) reflections were visible for the $R\bar{3}m$ NMC structure for the pristine sample. After cycling, the cells were extracted in an Ar-filled glove box and covered with Kapton tape to prevent air exposure. The Kapton tape introduced a background signal which is highlighted in Figure 3 and can be seen in the XRD spectrum of a bare substrate coated with Kapton tape in Figure S4. The (003) peak intensity is reduced after cycling for both the liquid and solid cells, although it is difficult to distinguish unambiguously due to the background signal from the Kapton. The (101) and (104) peaks are completely lost for the liquid cells, after 22 cycles, whereas the solid cells retained the (104) diffraction peak after cycling over 100 cycles although the intensity was significantly reduced. This is particularly interesting when considering the (104) plane. The (104) plane was found to be key to enabling good performance of thin films of NMC622 by allowing facile Li diffusion into the bulk compared to the (003) plane which inhibits intercalation.¹² The degradation of these favored (104) grains explains the massive capacity loss observed in these films due to reordering into an amorphous or disordered rock salt phase, as

suggested in literature.¹⁹ Despite the aggravated structural degradation of the NMC cathode in a liquid cell, the stable discharge capacity is still essentially the same. A conventional interpretation in literature is that this structural degradation is solely caused by Ni²⁺ ions migrating from octahedral 3a sites of the R $\bar{3}m$ structure into Li⁺ octahedral 3b sites at high states of delithiation due to similar ionic radii (0.69 and 0.76 Å, respectively).²⁰ This data supports previous work that observed that capacity loss is due to structural rearrangement. However, this work also suggests that oxygen redox catalyzed by the carbonate electrolyte could be an additional mechanism for this degradation. Indeed, given that the structure has not totally decomposed in the solid-state configuration, this would indicate electrolyte plays a critical role in the cathode degradation. The degraded crystal structure is responsible for the massive capacity loss on the first cycle for both the solid and liquid cells. This accounts for the similar specific discharge capacities observed in both configurations, as available Li storage sites were lost from the host NMC structure in both cases at high rates (17 mA/g).

Furthermore, the use of a stable high voltage solid electrolyte did not significantly improve capacity retention, which is contrary to a prevailing hypothesis in literature that stabilizing the CEI in liquid carbonate cells will enable good performance of Ni-rich NMC at high voltage. Interestingly, upon returning to low charge rates (5 mA/g) the capacity of the solid-state configuration increased to almost 79 mAh/g. This is consistent with the structural retention evident in the XRD data showing the retention of a significant fraction of the (104) texture. Our hypothesis is the cathode degradation occurs at the surface but helps kinetically passivate the core of the cathode structure by slowing further reactions. The newly amorphous cathode layer impedes Li transport at fast rates (17 mA/g) but at slower charge rates Li-ions can diffuse resulting in the observed capacity increase. In the liquid electrolyte case, we believe the cathode structural rearrangement at the surface is still not suitably passivating to overcome the promoting effect of the liquid electrolyte (discussed below) with respect to the kinetics of the cathode amorphization. This data is consistent with recent work demonstrating polymer coatings and thin metal oxide coatings which generated simple metal fluoride surface species during cycling and are correlated with increased capacity retention and lower interfacial impedance of these cathodes.¹⁷

Despite the importance of this finding, there is a significant discrepancy between the high voltage operation using the thin film cathodes presented here and that of the composite cathodes with a

traditional liquid electrolyte. Whereas structural degradation does occur within the composite cathodes the degradation is not near as quick or dramatic as for our thin film cathodes presented here. In the literature, one proposed mechanism for structural degradation of NMCs is that EC bonds with the cathode surface oxygen atoms of NMC622 as part of its dissociation reaction. This reaction was found to have lower activation energy for edge on planes of NMC333 and LiCoO_2 with EC²¹ such as the preferential orientation of the (104) planes of the thin films studied here. This orientation lowers the activation energy for this reaction because lattice oxygen atoms are exposed at the surface rather than predominantly transition metals or Li as would be the case for (003) planes lying parallel to the substrate.²¹ Oxygen vacancies in the crystal structure during EC decomposition can then form disordered rock salt and amorphous structures.²⁰ This preferential degradation along the (104) and (101) faces could explain why our cathodes degrade so quickly and could explain why the (104) plane degradation is worse in the liquid electrolyte than the solid electrolyte. It could also be the reason why what appears to be an irreversible oxygen redox plateau is observed only for liquid cells. This solution driven rearrangement lowers the activation energy for the structural rearrangement whereas the solid electrolyte blocks this pathway. But it cannot explain why the structural degradation and capacity loss still occurs when there is no EC available to catalyze the degradation.

Another key difference between a traditional NMC cathode and this cathode is the size and distribution of the crystallites. In a traditional NMC composite the active material is typically made up of polycrystalline particles a few microns in diameter with randomly oriented crystallites. In our cathodes the crystal structure is heavily influenced by the substrate resulting in the preferential orientation we observe in the XRD pattern. The full width half maximum of the (003) and (104) peaks also suggest that the crystal structure is unusual. The (003) peak (Figure S4) has a relatively low intensity relative to the (104) peak but is relatively sharp suggesting larger crystallite domains. The (104) peak on the other hand is relatively broad suggesting a much larger number of smaller crystallite domain sizes. This unusual crystallite morphology could be the reason for the extremely fast cathode degradation and capacity loss. Nonetheless, the conclusion that the stable solid-state electrolyte will not prevent structural degradation from occurring is very likely also true for a more traditional composite cathode design that also utilizes solid-state electrolytes.

Another key conclusion is the evidence for suppression of oxygen reduction when using a solid-state electrolyte. This correlates with the oxygen redox plateau present only during the first cycle of the liquid cells. The presence of the high voltage electrolyte effectively inhibited this behavior to produce a voltage profile which more closely aligns with literature on composite NMC622 electrodes. Our data also suggests that the preferential 104 orientation may aggravate this oxygen reduction as we see a much more pronounced oxygen reduction plateau compared to most literature reports with composite cathode. This also helps explain the disagreement in literature with regards to whether reactive oxygen species are present at the NMC surface during high voltage cycling. For example, Gasteiger's group hypothesized that singlet oxygen species evolve from the NMC lattice at high states of charge when the structure decomposes, driving electrolyte decomposition through chemical oxidation of ethylene carbonate.² While the results of this work cannot ascribe the oxygen redox to singlet oxygen formation, they do support the oxygen activity driven by high voltage operation. The partially reversible oxygen redox which is only observed on the first cycle might be explained by consumption of those active oxygen species by reaction with the electrolyte, contributing to the observed impedance rise and lower capacity due to CEI growth and aggravated structural degradation when compared to the solid-state case. As our data does seem to support the modeling work suggesting the (104) and (101) planes are particularly prone to this degradation, controlling the surface termination along these planes may help mitigate the structural degradation. However, we can additionally conclude that although the oxygen evolution may aggravate the structural decomposition of the electrode, it is not the root cause of this degradation.

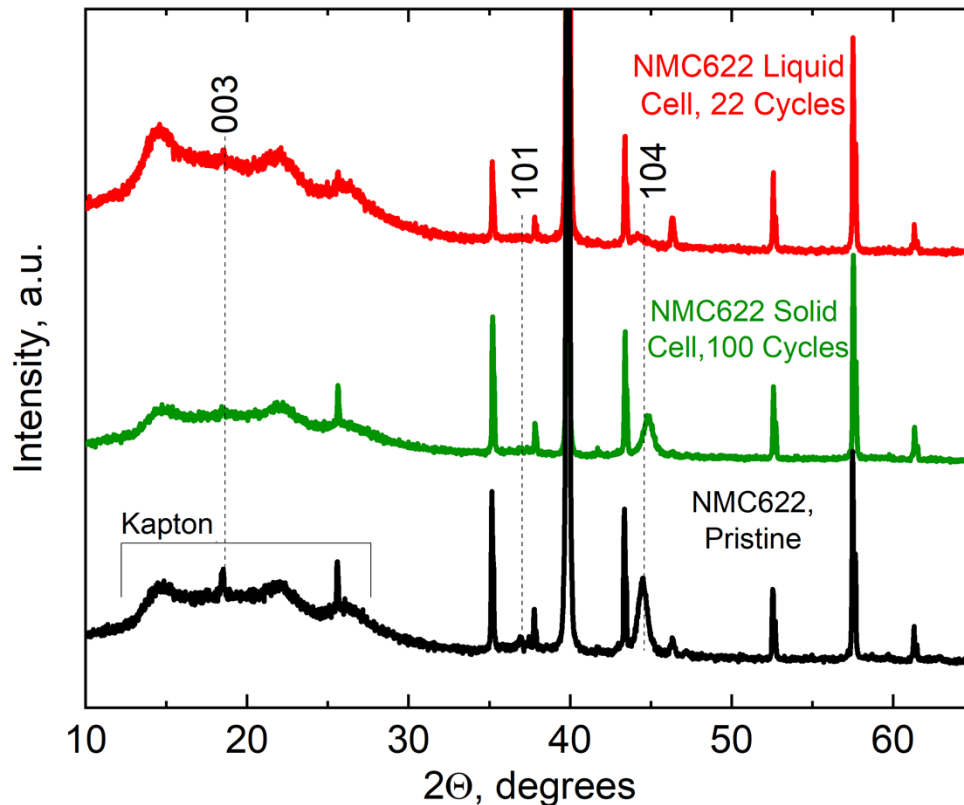


Figure 3. XRD of pristine 1.5 μm solid state NMC622 electrode and after 100 cycles at 10 mA/g. The cycled cell had a 1.7 μm layer of Lipon, 3 μm of Li, and Kapton tape on top of the NMC622. The cycled cathode from the liquid cell was also coated with Kapton tape after extraction. These data were normalized to the Al_2O_3 substrate peak at 57.6° for comparison.

CONCLUSIONS

Despite the interest in developing high voltage Ni-rich NMC solid state cells with high energy density, intrinsic limitations of the cathode with a (104) orientation were observed in this study. Both the solid-state cells and conventional liquid carbonate electrolyte cells exhibited severe capacity loss after the first charge cycle to 4.5 V vs. Li/Li^+ due to structural failure. The liquid cell continuously consumed electrolyte until cell failure while the solid-state cell remained stable albeit with a lower capacity. The thin film system used here resolves the ambiguity of studying composite electrodes and demonstrates that the initial capacity loss of NMC622 is decoupled from the cathode electrolyte interface, as both the continuously reacting interface in the liquid cell and the

stable interface in the solid cell had the same discharge capacities. This bulk structural degradation was not prevented by a stable CEI from a high voltage electrolyte (Lipon). Moving forward a clear study determining if the unusual crystallite morphology and preferential orientation is at the root of this structural degradation or if this is completely inherent to the NMC architecture when used at high voltage needs to be determined.

ASSOCIATED CONTENT

AUTHOR INFORMATION

*Corresponding authors' emails: nathandphillip@gmail.com, veithgm@ornl.gov

Notes – The authors declare no competing financial interest.

ORCID

Nathan D. Phillip: 0000-0002-6223-8765

Andrew S. Westover: 0000-0002-5738-1233

Claus Daniel: 0000-0002-0571-6054

Gabriel M. Veith: 0000-0002-5186-4461

ACKNOWLEDGMENTS

This research at the Oak Ridge National Laboratory, managed by UT Battelle, LLC, for the U.S. Department of Energy (DOE) under contract DE-AC05-00OR22725, was sponsored by the Office of Energy Efficiency and Renewable Energy (EERE) Vehicle Technologies Office (VTO) (Deputy Director: David Howell) Applied Battery Research subprogram (Program Manager: Peter Faguy) (N.D.P., C.D., and G.M.V.). Funding for A.S.W. was provided by ARPA-E Award No. DE-AR0000775.

REFERENCES

1. Manthiram, A., X. Yu, and S. Wang, *Lithium battery chemistries enabled by solid-state electrolytes*. Nature Reviews Materials, 2017. **2**: p. 16103.
2. Jung, R., M. Metzger, F. Maglia, C. Stinner, and H.A. Gasteiger, *Chemical versus Electrochemical Electrolyte Oxidation on NMC111, NMC622, NMC811, LNMO, and Conductive Carbon*. J Phys Chem Lett, 2017. **8**: p. 4820-4825.
3. Tian, C., Y. Xu, D. Nordlund, F. Lin, J. Liu, Z. Sun, Y. Liu, and M. Doeff, *Charge Heterogeneity and Surface Chemistry in Polycrystalline Cathode Materials*. Joule, 2018. **2**: p. 464-477.
4. Li, J., C. Ma, M. Chi, C. Liang, and N.J. Dudney, *Solid Electrolyte: the Key for High-Voltage Lithium Batteries*. Advanced Energy Materials, 2015. **5**.
5. Koerver, R., I. Aygün, T. Leichtweiß, C. Dietrich, W. Zhang, J.O. Binder, P. Hartmann, W.G. Zeier, and J. Janek, *Capacity Fade in Solid-State Batteries: Interphase Formation and Chemomechanical Processes in Nickel-Rich Layered Oxide Cathodes and Lithium Thiophosphate Solid Electrolytes*. Chem. Mater., 2017. **29**: p. 5574-5582.
6. Zhang, Z., S. Chen, X. Yao, P. Cui, J. Duan, W. Luo, Y. Huang, and X. Xu, *Enabling high-areal-capacity all solid-state lithium-metal batteries by tri-layer electrolyte architectures*. Energy Storage Materials, 2019.
7. Yoshinari, T., R. Koerver, P. Hofmann, Y. Uchimoto, W.G. Zeier, and J.r. Janek, *Interfacial stability of phosphate-NASICON solid electrolytes in Ni-rich NCM cathode-based solid-state batteries*. ACS applied materials & interfaces, 2019.
8. Ates, T., M. Keller, J. Kulisch, T. Adermann, and S. Passerini, *Development of an all-solid-state lithium battery by slurry-coating procedures using a sulfidic electrolyte*. Energy Storage Materials, 2019. **17**: p. 204-210.
9. Wang, D., Q. Sun, J. Luo, J. Liang, Y. Sun, R. Li, K. Adair, L. Zhang, R. Yang, S.J.A.a.m. Lu, and interfaces, *Mitigating the Interfacial Degradation in Cathodes for High-Performance Oxide-Based Solid-State Lithium Batteries*. 2019. **11**: p. 4954-4961.
10. Koerver, R., W. Zhang, L. de Biasi, S. Schweidler, A.O. Kondrakov, S. Kolling, T. Brezesinski, P. Hartmann, W.G. Zeier, and J. Janek, *Chemo-mechanical expansion of lithium electrode materials—on the route to mechanically optimized all-solid-state batteries*. Energy & Environmental Science, 2018. **11**: p. 2142-2158.
11. Dudney, N.J., *Solid-state thin-film rechargeable batteries*. Materials Science and Engineering: B, 2005. **116**: p. 245-249.
12. Phillip, N.D., R.E. Ruther, X. Sang, Y. Wang, R.R. Unocic, A.S. Westover, C. Daniel, and G.M. Veith, *Synthesis of Ni-Rich Thin-Film Cathode as Model System for Lithium Ion Batteries*. ACS Applied Energy Materials, 2019. **2**: p. 1405-1412.
13. Phillip, N.D., R.E. Ruther, X. Sang, Y. Wang, R.R. Unocic, A.S. Westover, C. Daniel, and G.M. Veith, *Synthesis of Ni-rich Thin Film Cathode as Model System for Lithium Ion Batteries*. ACS Applied Energy Materials, 2019.
14. Jung, R., M. Metzger, F. Maglia, C. Stinner, and H.A. Gasteiger, *Oxygen Release and Its Effect on the Cycling Stability of $\text{LiNi}_x\text{Mn}_y\text{Co}_z\text{O}_2$ (NMC) Cathode Materials for Li-Ion Batteries*. J. Electrochem. Soc., 2017. **164**: p. A1361-A1377.
15. Tian, C., D. Nordlund, H.L. Xin, Y. Xu, Y. Liu, D. Sokaras, F. Lin, and M.M. Doeff, *Depth-Dependent Redox Behavior of $\text{LiNi}_{0.6}\text{Mn}_{0.2}\text{Co}_{0.2}\text{O}_2$* . J. Electrochem. Soc., 2018. **165**: p. A696-A704.
16. Kim, Y., G.M. Veith, J. Nanda, R.R. Unocic, M. Chi, and N.J. Dudney, *High voltage stability of LiCoO_2 particles with a nano-scale Lipon coating*. Electrochim. Acta, 2011. **56**: p. 6573-6580.
17. Phillip, N.D., C. Daniel, and G.M. Veith, In Preparation, 2019.
18. Eliaz, N. and E. Gileadi, *Physical Electrochemistry: Fundamentals, Techniques, and Applications*. 2018: Wiley-Vch.
19. Dahn, J., U. von Sacken, and C.J.S.S.I. Michal, *Structure and electrochemistry of $\text{Li}_{1\pm y}\text{NiO}_2$ and a new Li_2NiO_2 phase with the Ni (OH) 2 structure*. 1990. **44**: p. 87-97.
20. Liu, W., P. Oh, X. Liu, M.J. Lee, W. Cho, S. Chae, Y. Kim, and J. Cho, *Nickel-rich layered lithium transition-metal oxide for high-energy lithium-ion batteries*. Angew. Chem. Int. Ed. Engl., 2015. **54**: p. 4440-57.

21. Xu, S., G. Luo, R. Jacobs, S. Fang, M.K. Mahanthappa, R.J. Hamers, and D. Morgan, *Ab Initio Modeling of Electrolyte Molecule Ethylene Carbonate Decomposition Reaction on Li(Ni,Mn,Co)O₂ Cathode Surface*. ACS Appl Mater Interfaces, 2017. **9**: p. 20545-20553.